Proton Conduction in a Phosphonate-based Metal-Organic Framework Mediated by Intrinsic "Free Diffusion Inside a Sphere"

Simona Pili,[1] Stephen P. Argent,[2] Christopher G. Morris,[2,3] Peter Rought,[1] Victoria García-Sakai,[4] Ian P. Silverwood,[4] Timothy L. Easun,[5] Ming Li,[6] Mark R. Warren,[3] Claire Murray,[3] Chiu C. Tang,[3] Sihai Yang,[1]* and Martin Schröder[1]*

[1] School of Chemistry, University of Manchester, Oxford Road, Manchester, M13 9PL (UK)
E-mail: Sihai.Yang@manchester.ac.uk; E-mail: M.Schroder@manchester.ac.uk
[2] School of Chemistry, University of Nottingham, University Park, Nottingham NG7 2RD (UK)
[3] Diamond Light Source, Harwell Science Campus, Oxfordshire, OX11 0DE (UK)
[4] ISIS Neutron Facility, STFC Rutherford Appleton Laboratory, Chilton, Oxfordshire, OX11 0QX (UK)
[5] School of Chemistry, Cardiff University, Cardiff, CF10 3XQ (UK)
[6]Department of Mechanical, Materials and Manufacturing Engineering, University of Nottingham, University Park, Nottingham NG7 2RD (UK)

ABSTRACT: Understanding the molecular mechanism of proton conduction is crucial for the design of new materials with improved conductivity. Quasi-elastic neutron scattering (QENS) has been used to probe the mechanism of proton diffusion within a new phosphonate-based metal-organic framework (MOF) material, MFM-500(Ni). QENS suggests that the proton conductivity (4.5 x 10^{-4} S cm^{-1} at 98% relative humidity and 25 °C) of MFM-500(Ni) is mediated by intrinsic "free diffusion inside a sphere", representing the first example of such a mechanism observed in MOFs.

Fuel cells represent an appealing option as alternative clean energy systems,[1] and technologies based upon polymer electrolyte membrane fuel cells (PEMFCs) are used widely in portable applications. The design and synthesis of new proton conducting materials are of fundamental importance for the development of PEMFCs,[2] and currently, the commercially used proton conductors are based upon acidic polymers such as Nafion which exhibit high conductivity of 10^{-2} S cm^{-1} in the presence of water.[3] However, the amorphous nature of such polymers precludes investigation of the mechanisms and/or pathways for their proton conduction, and thus analysis and feedback in order to improve future materials development are difficult to obtain.[4] Constructed from metal ions and organic linkers, metal-organic framework (MOF) materials often display high surface areas, high porosity and, more importantly, extended crystalline structures, and significant focus has been placed on their applications in gas storage, separation and catalysis.[5–7] More recently, MOFs have appeared as promising new candidates as porous materials for proton conduction.[8,9]

The functionalisation of the organic linker in MOF materials allows the periodic introduction of acidic groups (*e.g.*, SO_3H, PO_3H_2),[10-12] and their intrinsic porosity enables the loading of additional protonic molecules (*e.g.*, imidazole, histamine) within the pore[13-15] to yield decorated materials with improved proton conductivity. Most importantly, the crystalline nature of MOFs provides an excellent platform to interrogate possible proton hopping and conduction pathways thus enabling the construction of structure-activity relationships, which cannot be achieved in polymer-based systems due to their intrinsic lack of long-range order.[1] X-ray crystallographic studies afford average positions of protons within the extended lattice, mostly on oxygen atoms from hydroxy groups or water molecules. These are often refined by a "riding model" and subject to large uncertainties inherent in these X-ray experiments. Understanding the dynamics of these active protons is of fundamental importance for the design of improved materials. However, gaining such information within porous lattices of MOFs is very challenging and knowledge on the dynamics for proton diffusion in MOFs is lacking. Herein, we describe the synthesis and crystal structures of two novel isostructural phosphonate-based MOFs, $[M_3(H_3L)_2(H_2O)_9(C_2H_6SO)_3]$ (M = Ni, Co; H_6L = benzene-1,3,5-*p*-phenylphosphonic acid), denoted as MFM-500(Ni) and MFM-500(Co), respectively (MFM = Manchester Framework Material). MFM-500(Ni) and MFM-500(Co) adopt 2D networks, in which the ligand is only 50% deprotonated ($H_6L \rightarrow H_3L^{3-}$) and bound to the metal ions. This affords free acidic protons from the partially protonated ligand within the lattices of these coordination complexes. The materials show proton conductivities of 4.5 x 10^{-4} [MFM-500(Ni)] and 4.4 x 10^{-5} S cm^{-1} [MFM-500(Co)] at 98% RH (relative humidity) and 25 °C. Single crystal X-ray structural analyses reveal a potential proton hopping pathway constructed from the free phosphonic acid groups and coordinated water molecules on the metal centres, subject to uncertainties as discussed above. More importantly, quasi-elastic neutron scattering (QENS) has been used to investigate the intrinsic mechanism of proton diffusion within MFM-500(Ni) and this study suggests that the proton conduction in MFM-500(Ni) is mediated by the model of "free

diffusion inside a sphere" rather than that of "jump diffusion between sites".

Benzene-1,3,5-*p*-phenylphosphonic acid, H_6L (Figure 1a), was synthesised following a literature procedure to afford a white powder in a 67% yield.[16] Upon mixing $M(NO_3)_2$ (M = Ni, Co) with H_6L in a 2:1 molar ratio in a solution of H_2O/DMSO/DMF, hexagonal column-shaped single crystals of MFM-500(Ni) and MFM-500(Co) grew within 2 days at 40 °C. Synchrotron single crystal X-ray diffraction reveals that the two materials are isostructural and both crystallise in the hexagonal space group $P6_3/m$ (Table S1) with a 2D layered structure. The *tris*-phosphonate ligand, H_3L^{3-}, acts as one type of three-connected node in overlapping pairs of 2-dimensional hexagonal (6,3) networks lying in the *ab* plane, in which the other type of three-connected node is a disordered mixture of $[M_1(H_2O)_3(RPO_3H)_3]$ or $[M_2(H_2O)_6(\mu^2\text{-}RPO_3H)_3]$ moieties (Figure 1b). Running down the *c*-axis are stacks of pairs of overlapping ligands in which each pair is rotated by 60° with respect to the pair above and below (ligand separations along the *c*-axis are 3.85 Å between overlapping pairs). Columns of disordered metal centres running along the *c*-axis all have pseudo-octahedral coordination geometries made up of oxygen donors from deprotonated phosphonate hydroxyl groups, neutral water molecules and partially resolved DMSO molecules. These oxygen donors act in either monodentate or μ²-bridging ligands depending on the occupancy of the disordered adjacent metal cation sites. The columns of M_1 and M_2 nodes along the *c*-axis reside in the hexagonal holes within the pairs of offset hexagonal networks above and below them (Figure 1c).

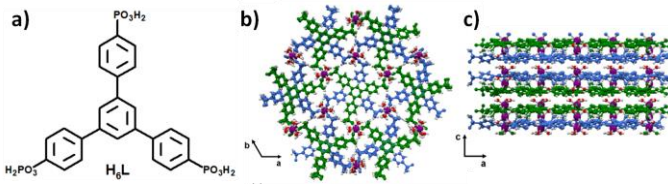

Figure 1. (a) Chemical structure of the ligand H_6L. Views of the crystal structure of MFM-500(M) (M = Co, Ni) along the *c*-axis (b) and along the *b*-axis (c). Minor disorder component sites and DMSO solvent molecules have been omitted for clarity. Overlapping stacks of ligands: blue and green, metal centers: purple, bridging water oxygen atoms: red, hydrogen atoms: white.

In MFM-500(Co), residual electron density peaks were observed for hydrogen atoms on the water molecules and one of the phosphonate hydroxy groups; this has allowed their positions to be refined using suitable geometric restraints revealing an extensive hydrogen bonding network within and between the columns of metal cations (Figure 2; Table 1). The hydrogen bond donor-acceptor distances range from 2.45 to 3.01 Å and form cross-over chains that run between adjacent columns of metal cations *via* reciprocally disordered hydrogen bonds between symmetry-related phosphonate-hydroxy oxygen atoms O33 (donor-acceptor distance 2.45 Å). The phosphonate-hydroxy oxygen atom O33 is also involved in disordered hydrogen bonding with a bridging water molecule O2W (donor-acceptor distance 2.73 Å), while the bridging water molecule O1W donates a bifurcated hydrogen bond to two symmetrically-equivalent unbound deprotonated phosphonate-hydroxy oxygen atoms O34 (donor-acceptor distance 3.01 Å). The passage of hydrogen bond chains along the *c*-axis is interrupted by the presence of a partially occupied disordered DMSO solvent molecule; it is likely that the chains continue through this region conveyed by an unmodelled disorder solvent component. Refinement of the crystal structure of MFM-500(Ni), however, yields no clear electron density peaks on the oxygen donors, thus precluding the inclusion of precise H positions within the model. The array of potential hydrogen bond donors and acceptors in MFM-500(Ni) is the same as that in MFM-500(Co), the separation between water oxygen O1W and phosphonate oxygen O34 being slightly shorter [D···A 3.3013(7) Å in MFM-500(Co) and 2.972(7) in MFM-500(Ni)]. The other donor-acceptor distances are similar (Table 1).

TGA (thermal gravimetric analysis) of MFM-500(Ni) and MFM-500(Co) show similar weight loss steps with a slightly lower stability observed for MFM-500(Co) (Figure S2a). *In situ* variable temperature PXRD data confirmed a reversible phase transition occurring between 75 and 100 °C for both materials (Tables S2, S3). This result is consistent with the first step in the TGA plots and is associated with a color change from green to brown for MFM-500(Ni) and from pink to purple for MFM-500(Co) (Figure S2b). The original phase

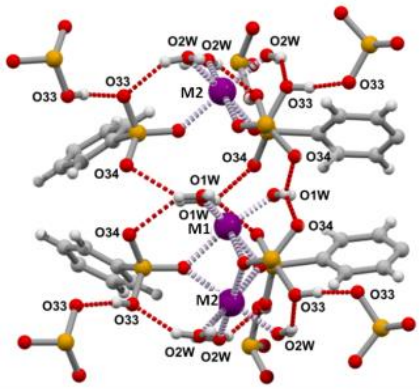

can be recovered by exposing the dehydrated samples to air (or water vapor), suggesting a reversible change in the coordinated water molecules upon dehydration/rehydration. This is further evidenced by the dehydrated samples remaining intact and stable under a flow of dry O_2. Due to the quality of the data and the complexity of these structures, attempts to determine the crystal structures of the dehydrated phases have thus far been unsuccessful.

Figure 2. View of the coordination environment of M_1 and M_2 and the surrounding hydrogen bond network from the single crystal X-ray structure of MFM-500(Co). Carbon atoms: grey, oxygen atoms: red, phosphorus atoms: orange, metal centers: purple, hydrogen atoms: white. Coordinate bonds are shown as dashed lilac lines, and hydrogen bonds are shown as dashed red lines.

Table 1 Summary of hydrogen bond distances in MFM-500(Co) and MFM-500(Ni).

D	H	A	MFM-500(Co) d(D-H)/Å	MFM-500(Co) d(H-A)/Å	MFM-500(Co) d(D-A)/Å	MFM-500(Co) D-H-A/°	MFM-500(Ni) d(D-A)/Å
O1W	H1WA	O34	0.843(10)	2.289(18)	3.013(7)	144(2)	2.972(7)
O1W	H1WA	O34[1]	0.843(10)	2.289(18)	3.013(7)	144(2)	2.972(7)
O2W	H2WA	O33[2]	0.839(10)	2.01(5)	2.726(6)	142(7)	2.716(5)
O33	H33A	O33[4]	0.840(10)	1.62(4)	2.453(7)	170(19)	2.483(7)
O33	H33	O2W[3]	0.838(10)	1.99(8)	2.726(6)	147(13)	2.716(5)

[1]+X,+Y,1/2-Z; [2]1-Y,1+X-Y,+Z; [3]+Y-X,1-X,+Z; [4]1-X,2-Y,1-Z

The proton conductivities of MFM-500(Ni) and MFM-500(Co) were studied by AC impedance spectroscopy. Nyquist plots contain an incomplete semi-circle in the high frequency region and a pronounced tail at low frequencies, consistent with blocking of protons at the electrodes (Figure 3a). At room temperature and 98 % RH, the proton conductivities for MFM-500(Ni) and MFM-500(Co) were measured as 4.5 x 10^{-4} and 4.4 x 10^{-5} S cm^{-1}, respectively. The difference in the conductivities between these isostructural materials probably correlates to the bond strength between coordinated water molecules and the metal cations, as suggested by the TGA plots and solid-state UV-visible absorption spectra (see SI). These values are comparable to those recently reported for MOFs functionalised with phosphonic acid groups under similar conditions. For example, GdHPA-II (HPA = 2-hydroxyphosphonoacetic acid) shows a proton conductivity of 3.2 x 10^{-4} S cm^{-1} at 21 °C and 98 % RH, while [Zn-(*m*-H_6L)] [*m*-H_6L = 1,3-*bis*(aminomethyl)benzene-*N*,*N*'-*bis*(methylenephosphonic acid)] has a proton conductivity of 1.4 x 10^{-4} S cm^{-1} at 41 °C and 98 % RH.[17] More recently, {[$(Me_2NH_2)_3(SO_4)$]$_2$[$Zn_2(ox)_3$]} and UiO66-SO_3H show higher proton conductivities of 4.2 x 10^{-2} S cm^{-1} at 25 °C and 98 % RH and 3.4 x 10^{-3} S cm^{-1} at 30 °C and 97 % RH, respectively.[18] Impedance data were also measured at 98 %, 75 %, 45 % and 0 % RH at 25 °C for MFM-500(Ni) and MFM-500(Co); both materials showed steady decrease of conductivity with the decreasing % RH (Figure S3 and S4, Table S4). At 0 % RH both materials showed no apparent conductivity (below 10^{-9} S cm^{-1}). This is typically observed for water-mediated proton conductors. It is worth noting that the dehydrated materials show no apparent proton conductivity and their conductivities (4.5 x 10^{-4} and 4.4 x 10^{-5} S cm^{-1} for the Ni and Co compounds, respectively) can be recovered by exposing the dehydrated samples to water vapor, consistent with the reversible phase change shown by the *in situ* PXRD data.

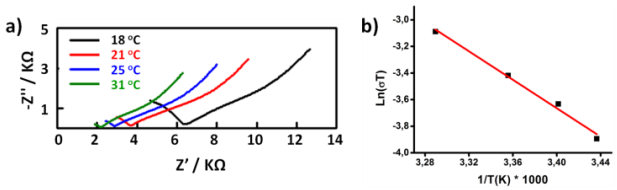

Figure 3. (a) Nyquist plot for MFM-500(Ni) measured at different temperatures and 98 % RH. (b) Arrhenius plot of the proton conductivity at various temperatures of MFM-500(Ni) under 98 % RH.

The activation energy of the proton conduction in MFM-500(Ni) was estimated from the impedance spectra recorded at 98 % RH between 18 and 31 °C to be 0.46 eV (Figure 3b). Two main mechanisms for proton diffusion are the Vehicle mechanism (typically E_a > 0.4 eV) and the Grotthuss mechanism (typically E_a < 0.4 eV).[8] The activation energy for MFM-500(Ni) lies at the boundary of the two mechanisms, indicating that it is likely that proton conduction in MFM-500(Ni) is governed by an intermediate process between the Grotthuss and Vehicle mechanisms. This behaviour has been reported in a few cases.[2,19,20] For example, $(NH_4)_2$(adp)[$Zn_2(ox)_3$]·$3H_2O$ (adp = adipic acid; ox^{2-} = oxalate) shows a high proton conductivity of 8 x 10^{-3} S cm^{-1} at 25 °C under 98 % RH with an E_a of 0.63 eV, and the mechanism of proton conduction was assigned as mixed Grotthuss and Vehicle types.[19,20]

We sought to gain further understanding of the mechanism of proton conduction in MFM-500(Ni) using quasi-elastic neutron scattering (QENS). Data for MFM-500(Ni) were collected between -23 to 150 °C under both anhydrous and 98% RH conditions to study the dynamics of protons through the framework lattice. The elastic incoherent structure factors, EISF, were extracted from the QENS spectra to gain the geometrical information of the molecular motions of active protons in MFM-500(Ni) (see SI). The EISF plots showed clear Q-dependence and were carefully fitted with all well-known theoretical models for proton diffusion (*i.e.*, jumping between *n* sides and various free diffusion models as shown in Figure S6). It has been found that the proton diffusion in MFM-500(Ni) is best described by the model of "free diffusion inside a sphere" (equation 1) rather than the model of jumping between *n* sites (Figure 4a and S6).[21-23]

$$EISF = p + (1-p) * [(3j_1(Qr)/(Qr)]^2 \qquad \text{(equation 1)}$$

where j_1 is the first order spherical Bessel function, *r* is the radius of the sphere, and p and (1-p) are the immobile and mobile fraction of the protons involved in this process, respectively. The radius of the "sphere", *r*, to host the proton diffusion was then "refined" by tuning it between 1.8 and 3.0 Å (Figure S7). The best fitting to the EISF plot was observed for *r* = 2.25 Å, entirely consistent with the observed H···A distances from the single crystal X-ray structure (taking an O-H bond distance of ~0.84 Å). The dependency of the spherical free diffusion on the distance *r* is confirmed by the extraction of the half-width of the half-maximum (HWHM, Γ) of the QENS spectra as a function of Q^2 at different temperatures (Figure 4b).[22,24] For Q^2 values greater than 1.95 $Å^{-2}$ (corresponding to $r \leq 2.25$ Å), Γ increases with Q^2 indicating free diffusion of protons within a distance of 2.25 Å. For Q^2 values below 1.95 $Å^{-2}$ (corresponding to $r > 2.25$ Å), Γ does not have any dependency on Q^2, suggesting a confined motion at distances beyond 2.25 Å. This is entirely reasonable because when the distances are longer than 2.25 Å, the proton conduction needs to be assisted by additional water molecules (or other vehicle molecules), *i.e.* the origin for the presence of the cooperated Grotthuss and Vehicle mechanisms. QENS data of MFM-500(Ni) recorded under humid conditions confirms that the proton diffusion remains as "free diffusion inside a sphere" with the same diffusion distance *r* of 2.25 Å (Figure S8).

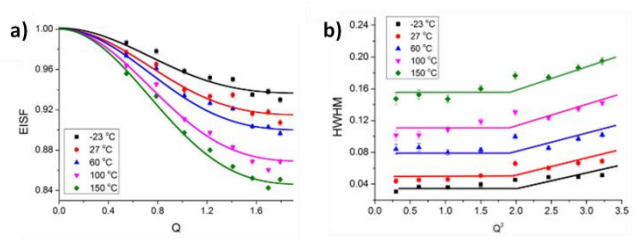

Figure 4. (a) View of the elastic incoherent structure factor (EISF) of MFM-500(Ni). Solid curves represent the simulated EISF based on function (equation 1) for the model of "free diffusion inside a sphere" at different temperatures. (b) Q^2-dependence of the half-width of the half-maximum (HWHM) estimated from the fitting of the data for MFM-500(Ni). Lines are a guide to the eye.

In conclusion, we have combined the single crystal X-ray diffraction and QENS spectroscopy to study the molecular mechanism for proton conduction in a new phosphonate-based MOF material. These complementary static and dynamic approaches yield highly consistent results and afford direct visualisation of the pathway and mechanisms of proton transfer in the framework lattice. For the first time, the model of "free diffusion inside a sphere" has been experimentally confirmed in proton-conducting MOFs. Further efforts to optimize the hydrogen bonding network in these materials *via* ligand modification and post-synthetic approaches are currently underway.

ASSOCIATED CONTENT

Supporting Information

Synthesis procedures, characterization, impedance analysis and QENS analysis. CCDC-1450010 and CCDC-1450011 contain the supplementary crystallographic data for this paper. The Supporting Information is available free of charge on the ACS Publications website at DOI: XX.XXX/jacs.XXXXXXX.

AUTHOR INFORMATION

Notes

The authors declare no competing financial interests.

Corresponding Author

Sihai.Yang@manchester.ac.uk;
M.Schroder@manchester.ac.uk

ACKNOWLEDGMENTS

We thank Universities of Manchester and Nottingham and EPSRC for funding. We are especially grateful to STFC and the ISIS Facility for access to Beamline IRIS, to Diamond Light Source for access to Beamlines I11 and I19. MS thanks the ERC for Advanced Grant.

REFERENCES

1. Yoon, M.; Suh, K.; Natarajan, S.; Kim, K. *Angew. Chem. Int. Ed.* **2013**, *52*, 2688–2700.
2. Liang, X.; Zhang, F.; Feng, W.; Zou, X.; Zhao, C.; Na, H.; Liu, C.; Sun, F.; Zhu, G. *Chem. Sci.* **2013**, *4*, 983–992.
3. (a) Tsai, C. H.; Wang, C. C.; Chang, C. Y.; Lin, C. H.; Yang, Y. W. *Int. J. Hydrogen Energ.* **2014**, *39*, 15696-15705. (b) Phang, W. J.; Jo, H.; Lee, W. R.; Song, J. H.; Yoo, K.; Kim, B. S.; Hong, C. S. *Angew. Chem. Int. Ed.*. **2015**, *54*, 5142–5146.
4. (a) Sahoo, S. C.; Kundu, T.; Banerjee, R. *J. Am. Chem. Soc.* **2011**, *133*, 17950–17958. (b) Taylor, J. M.; Mah, R. K.; Moudrakovski, I. L.; Ratcliffe, C. I.; Vaidhyanathan, R.; Shimizu, G. K. H. *J. Am. Chem. Soc.* **2010**, *132*, 14055–14057. (c) Taylor, J. M.; Dawson, K. W.; Shimizu, G. K. H. *J. Am. Chem. Soc.* **2013**, *135*, 1193–1196.
5. (a) Yang, W.; Lin, X.; Jia, J.; Blake, A. J.; Wilson, C.; Hubberstey, P.; Champness, N. R.; Schröder, M. *Chem. Commun.* **2008**, *3*, 359–361. (b) Jia, J.; Lin, X.; Wilson, C.; Blake, A. J.; Champness, N. R.; Hubberstey, P.; Walker, G.; Cussen, E. J.; Schröder, M. *Chem. Commun.* **2007**, *3*, 840–842. (c) Suh, M. P.; Park, H. J.; Prasad, T. K.; Lim, D. *Chem. Rev.* **2012**, *112*, 782–835. (d) Dailly, A.; Poirier, E. *Energy Environ. Sci.* **2011**, *4*, 3527–3534. (e) Yan, Y.; Lin, X.; Yang, S.; Blake, A. J.; Dailly, A.; Champness, N. R.; Hubberstey, P.; Schröder, M. *Chem. Commun.* **2009**, *9*, 1025–1027. (f) Farha, O. K.; Yazaydın, A. Ö.; Eryazici, I.; Malliakas, C. D.; Hauser, B. G.; Kanatzidis, M. G.; Nguyen, S. T.; Snurr, R. Q.; Hupp, J. T. *Nature Chem.* **2010**, *2*, 944–948. (g) Yan, Y.; Telepeni, I.; Yang, S.; Lin, X.; Kockelmann, W.; Dailly, A.; Blake, A. J.; Lewis, W.; Walker, G. S.; Allan, D. R.; Barnett, S. A; Champness, N. R.; Schröder, M. *J. Am. Chem. Soc.* **2010**, *132*, 4092–4094.
6. Yang, S.; Sun, J.; Ramirez-Cuesta, A. J.; Callear, S. K.; David, W. I. F.; Anderson, D. P.; Newby, R.; Blake, A. J.; Parker, J. E.; Tang, C. C.; Schröder, M. *Naure Chem.* **2012**, *4*, 887–894.
7. Li, J.; Sculley, J.; Zhou, H. *Chem. Rev.* **2012**, *112*, 869–932.
8. Ramaswamy, P.; Wong, N. E.; Shimizu, G. K. H. *Chem. Soc. Rev.* **2014**, *43*, 5913–5932.
9. Horike, S.; Umeyama, D.; Kitagawa, S. *Acc. Chem. Res.* **2013**, *46*, 2376–2384.
10. Shigematsu, A.; Yamada, T.; Kitagawa, H. *J. Am. Chem. Soc.* **2011**, *133*, 2034–2036.
11. Kim, S.; Dawson, K. W.; Gelfand, B. S.; Taylor, J. M.; Shimizu, G. K. H. *J. Am. Chem. Soc.* **2013**, *135*, 963–966.
12. Bazaga-Garcia, M.; Colodrero, R. M. P.; Papadaki, M.; Garczarek, P.; Zon, J.; Olivera-pastor, P.; Losilla, E. R.; Leo, L.; Aranda, M. A. G. *J. Am. Chem. Soc.* **2014**, *136*, 5731–5739.
13. Bureekaew, S.; Horike, S.; Higuchi, M.; Mizuno, M.; Kawamura, T.; Tanaka, D.; Yanai, N.; Kitagawa, S. *Nature Mater.* **2009**, *8*, 831–836.
14. (a) Hurd, J.; Vaidhyanathan, R.; Thangadurai, V.; Ratcliffe, C. I.; Moudrakovski, I. L.; Shimizu, G. K. H. *Nature Chem.* **2009**, *1*, 705–710. (b) Umeyama, D., Horike, S., Inukai, M.; Kitagawa, S. *J. Am. Chem. Soc.* **2013,** *135*, 11345–11350.
15. Liu, S.; Yue, Z.; Liu, Y. *Dalton Trans.* **2015**, 12976–12980.
16. Beckmann, J.; Rüttinger, R.; Schwich, T. *Cryst. Growth Des.* **2008**, *8*, 3271–3276.
17. (a) Colodrero, R. M. P.; Papathanasiou, K. E.; Stavgianoudaki, N.; Olivera-Pastor, P.; Losilla, E. R.; Aranda, M. A. G.; León-Reina, L.; Sanz, J.; Sobrados, I.; Choquesillo-Lazarte, D.; García-Ruiz, J. M.; Atienzar, P.; Rey, F.; Demadis, K. D.; Cabeza, A. *Chem. Mater.* **2012**, *24*, 3780–3792. (b) Colodrero, R. M. P.; Angeli, G. K.; Bazaga-Garcia, M.; Olivera-Pastor, P.; Villemin, D.; Losilla, E. R.; Martos, E. Q.; Hix, G. B.; Aranda, M. A. G.; Demadis, K. D.; Cabeza, A. *Inorg. Chem.* **2013**, *52*, 8770–8783.
18. (a) Nagarkar, S. S.; Unni, S. M.; Sharma, A.; Kurungot, S.; Ghosh, S. K. *Angew. Chem.* **2014**, *53*, 2638–2642. (b) Phang, W. P.; Jo, H.; Lee, W. R.; Song, J. H.; Yoo, K.; Kim, B. S.; Hong, C. S. *Angew. Chem. Int. Ed.* **2015**, *54*, 5142-5146.

19. Sadakiyo, M.; Yamada, T.; Kitagawa, H. *J. Am. Chem. Soc.* **2009**, *131*, 9906–9907.
20. Sadakiyo, M.; Yamada, T.; Kitagawa, H. *J. Am. Chem. Soc.* **2014**, *136*, 13166–13169.
21. Russo, D.; Pérez, J.; Zanotti, J.-M.; Desmadril, M.; Durand, D. *Biophys. J.* **2002**, *83*, 2792–2800.
22. Volino, F.; Dianoux, A. *J., Mol. Phys.* **1980**, *41*, 271.
23. Bee, M. "*Quasielastic Neutron Scattering*" **1988**.
24. Mukhopadhyay, R.; Mitra, S. *Indian J. Pure Appl. Phys.* **2006**, *44*, 732–740.